TECHNICAL UNIVERSITY OF CLUJ-NAPOCA

ACTA TECHNICA NAPOCENSIS

Series: Applied Mathematics, Mechanics, and Engineering
Vol. 65, Issue Special III, November, 2022

STUDY ON THE IMPLEMENTATION OF AN ALTERNATIVE SOLUTION TO THE CURRENT IRRIGATION SYSTEM

Dorin BORDEAȘU

Abstract: *In the current paper is presented a technical and economic study for integrating a high-power photovoltaic generator into an existing irrigation system. In the first part the modelling of each component of the existing irrigation system is presented (Hydraulic network, submersible pump, induction motor and the diesel generator). In the second part the modelling of a high-power generator on a horizontal axis N-S solar tracker. Finally, in the last part the payback period of the high-power PV generator is calculated, considering just the price of the diesel used by the generator to extract and pump the same volume of water.*
Key words: *High-power photovoltaic generator, Photovoltaic irrigation system, Photovoltaic pumping system, Economic and technical study, Diesel generator.*

1. INTRODUCTION

In the last decade, more and more irrigation systems have been upgraded with sprinklers, or drip irrigation systems, for increasing the water usage efficiency. Due to this reason, the energy consumption by the irrigation systems increased drastically leading to such a cost of the energy consumption, that nowadays, represents the highest cost in operating an irrigation system. The irrigation systems used in agriculture, are supplied with electricity either from the national grid either by a gasoline or diesel electric generators depending on which one was more economically at the system execution.

The continuing price rise of the gasoline, diesel and electricity, makes the agricultural sector looking more and more into alternatives sources of electricity such as renewable ones due to their stable price and reduced low CO2 emissions.

Even though there are some irrigation systems powered by wind generators because of their high availability (more than 2400 working hours/year), the photovoltaic generators represent a better integration into an irrigation system, because those systems produce most of the energy exactly during irrigation period (during the summer, with maximum demand in the hottest and sunniest days of the year).

Given the above, the current paper proposes a methodology for evaluating the technical and economic possibility for integrating a photovoltaic generator into an existing irrigation system by determining the characteristics of the photovoltaic generator based on the energy requirements of the existing irrigation system. In the current paper, it is deeply described how to dimension the photovoltaic generator, determine the characteristics of the electrical power converter, design the distribution system with its adequate protection, and calculate the payback period of integrating a photovoltaic generator into an irrigation system.

2. EXISTING IRRIGATION SYSTEM

The existing irrigation system is in Aragon region in Spain (Lat=latitude), and it is used for direct irrigation of tree fruit orchards. In Figure 1, it can be seen its layout and the main components of the existing irrigation system (black drawing line): a diesel generator, powering an induction motor connected to a submersible pump that extracts the water from a well and distribute it into an irrigation network.

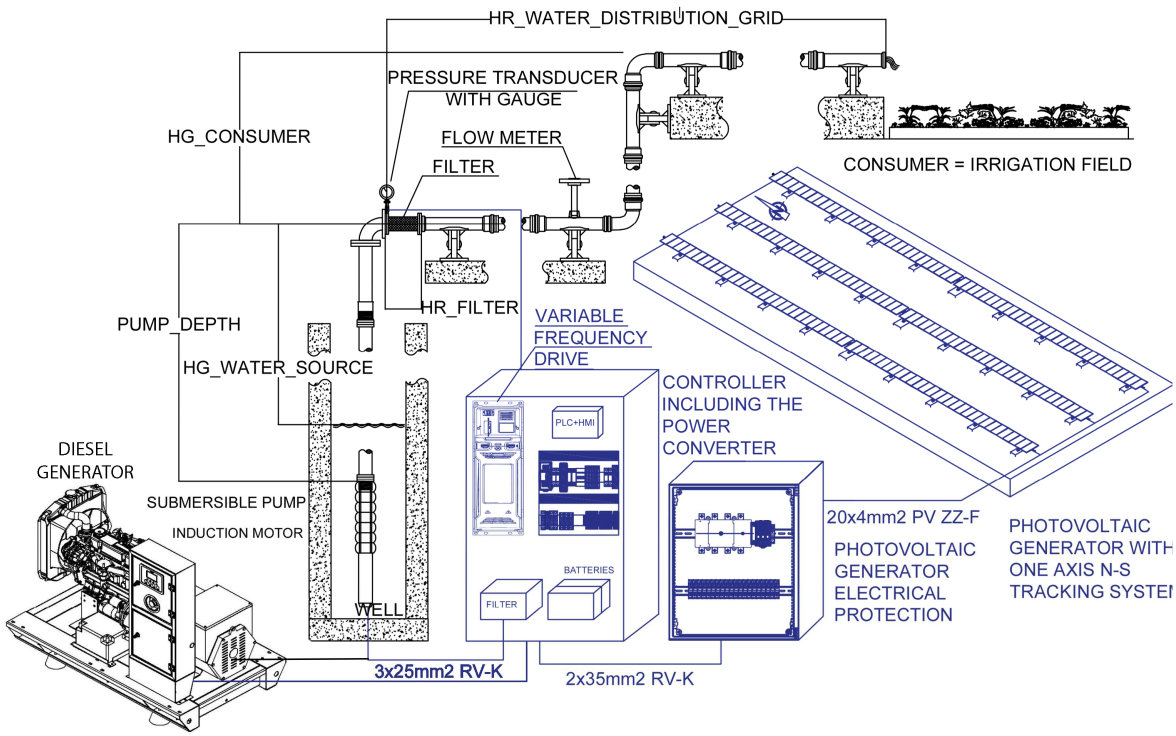

Fig. 1. Irrigation system diagram.

2.1. Water needs

In Table 1, it is presented the average operation during each day of the month of the existing irrigation system, according to the user.

Based on operating hours/day each month from Table 1, and the measured operating flow 85m^3/h, the water volume pumped into the irrigation system each month was calculated in Table 2.

Table 1

Operating period of the actual irrigation system.

Month	Operating hours/day	Operating days/ month
January	0	0
February	0	0
March	10,5	12
April	14	20
May	14	31
June	17,5	30
July	17,5	31
August	17,5	31
September	17,5	20
October	0	0
November	0	0
December	0	0

Table 2

Water volume pumped into the irrigation system.

Month	Water volume pumped each day	Water volume pumped each month
January	0	0
February	0	0
March	892.5	10710
April	1190	23800
May	1190	36890
June	1487.5	44625
July	1487.5	46112.5
August	1487.5	46112.5
September	1487.5	29750
October	0	0
November	0	0
December	0	0
Total pumped volume/year		177 442 m^3

2.2 Hydraulic network

The hydraulic network consists in 55 m of a vertical well steel pipe (diameter of 30 cm), a mesh filter, 1000 m of horizontal distribution PP pipe (diameter of 30 cm), and other elements as tees, 45- and 90-degrees elbows, and 5 sectors equivalent sectors with approximately 6000 meters of drip irrigation system each, working with a pressure range between 1.5 to 2.5 bars. In Figure. 2 it can be seen the hydraulic network characteristic curve.

The water distribution and irrigation system characteristic curve are expressed by equation [1]:

$$H_o = Hg + k \cdot (Q_0)^2 \qquad (1)$$

where Hg is the static head (HG_WATER_SOURCE≈ 40 m + HG_CONSUMER in Figure 1), Q_o is the pump operating flow rate, and k is the head loss coefficient.

The nominal hydraulic power required for operating the irrigation system is estimated according to the following equation [2]:

$$P_{hid0} = \rho \cdot g \cdot H_0 \cdot Q_0 \qquad (2)$$

2.3 Submersible pump

A submersible pump [3], collects the water from a well and distributes it into an irrigation hydraulic network. The pump is installed at a depth of 80 m below the ground level (PUMP_DEPTH≈ 80 m in Figure. 1), and the water dynamic level is 40 m (HG_WATER_SOURCE≈ 40 m in Figure 1). The maximum extractable flow from the well is 95 m3/h. but the pump operates at the nominal flow of 85 m3/h. In Figure 2 it can be seen the iso-efficiency diagram of the submersible pump.

The pump is modeled based on A, B, and C coefficients identified through quadratic regression (2) from the centrifugal pump characteristic head–flow (Hn-Qn) curve, and on D and E coefficients also identified through quadratic regression (10) from the efficiency–flow (ηn-Qn) curve. Both curves (Hn-Qn and ηn-Qn) are at nominal speed (ωn) [1,4,5]. Starting from Equation (3), the subscript “0” stands for the nominal values.

$$H_0 = A + B \cdot Q_0 + C \cdot (Q_0)^2 \qquad (3)$$

$$\eta_{p0} = D \cdot Q_0 + E \cdot (Q_0)^2 \qquad (4)$$

where H_0 represents the nominal pump head, Q_0 the nominal pump flow, and η_{p0} the nominal pump efficiency.

Table 3

Submersible pump characteristics [3].

Submersible pump data	Value
Submersible pump pipe diameter	0.2 m
Ambient temperature	35 °C
Minimum water speed to cool the jacket of the motor	0.5 m/s
Maximum number of starts in one hour	20
Minimum immersion depth	507,5 m
Submersible pump service flow rate	91.85 m3/h
Submersible pump service head	78.12 m
Submersible pump efficiency	75.63 %
Submersible pump hydraulic power	25.84 kW
Submersible pump maximum flow rate	169.2 m3/h
Submersible pump head at theoretical 0 flow rate	97.35 m
Submersible pump minimum head (at maximum flow rate)	83.29 m
Submersible pump efficiency at maximum flow rate	81.5 %
Submersible pump hydraulic power at maximum flow rate	30 kW

It will be denoted with α α=ω/ω0 the ratio between the pump operating angular velocity (ω), and the nominal angular velocity (ω0).

The response of the centrifugal pump to a different speed is modeled using the pump affinity laws (in the current work, the change in water density ρwo=ρwn and pump geometry Go=Gn during the speed variation are ignored) [6, 7 (p. 776)]:

$$\frac{Q}{Q_0} = \frac{\omega}{\omega_0} \cdot \left(\frac{G}{G_0}\right)^3 = \alpha \qquad (5)$$

$$\frac{H}{H_0} = \left(\frac{\omega}{\omega_0}\right)^2 \cdot \left(\frac{G}{G_0}\right)^2 = \alpha^2 \qquad (6)$$

$$\frac{P_1}{P_{10}} = \frac{\rho_w}{\rho_{w0}} \cdot \left(\frac{\omega}{\omega_0}\right)^3 \cdot \left(\frac{G}{G_0}\right)^3 = \alpha^3 \qquad (7)$$

where P stands for the pump power consumption.

By combining the (H0-Q0) quadratic regression Equation (3) at nominal speed (ω0) with the pump affinity laws, Equation (5-7), the pump characteristic (H-Q) as a function of pump speed is obtained (7):

$$H = \alpha^2 \cdot A + \alpha \cdot B \cdot Q + C \cdot (Q)^2 \quad (8)$$

Figure 2 shows the pump characteristic (H-Q) curve at different speeds (frequency variation from 5 to 50 Hz). The data sheet of the submersible pump can be found in reference [3].

$$\eta_p = 1 - \left[1 - D \cdot \frac{Q}{\alpha} - E \cdot \left(\frac{Q}{\alpha}\right)^2\right] \cdot \left(\frac{1}{\alpha}\right)^{0.1} \quad (13)$$

$$\eta_p = 1 - \frac{1}{\alpha^{0.1}} + \frac{D \cdot Q}{\alpha^{1.1}} + \frac{E \cdot Q^2}{\alpha^{2.1}} \quad (14)$$

By substituting the nominal head (H0) and flow (Q0) of the pump in equation 2, with the actual operating head (H) and flow of the pump

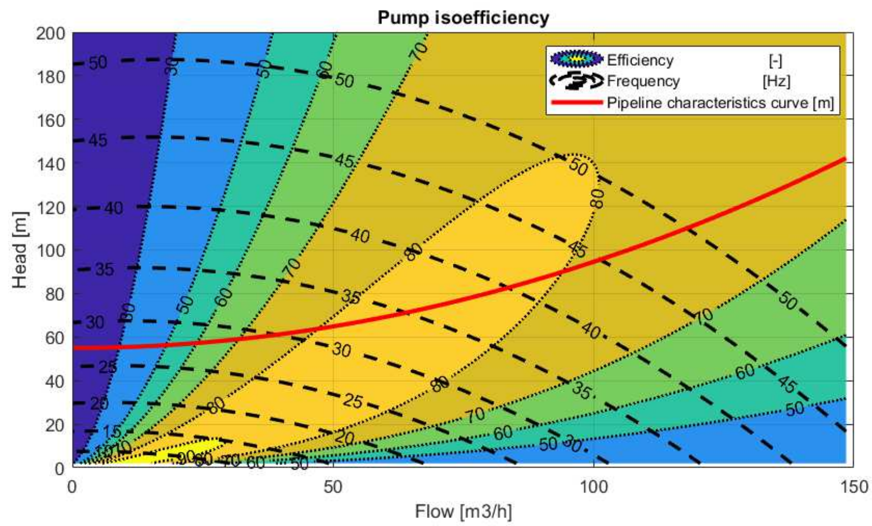

Fig. 2. Pump isoeffieceincy curve together with the hydraulic network characteristic curve (Ho-Qo-ηo).

The delivered flow as a function of pump speed (ω) is given by the pump operating point, represented by the cross-point of the pump characteristic (8) with the system characteristic curve (1):

$$H_g + k \cdot Q^2 = \alpha^2 \cdot \mathrm{A} + \alpha \cdot \mathrm{B} \cdot \mathrm{Q} + C \cdot Q^2 \quad (9)$$

From which results:

$$\alpha = \frac{BQ - \sqrt{B^2 \cdot \mathrm{Q}^2 - 4A\left[(C-k) \cdot \mathrm{Q}^2 - \mathrm{H_g}\right]}}{2 \cdot A} \quad (10)$$

In the current paper, the pump efficiency at partial load, it is calculated using reference [4].

By combining the (ηp0-Q0) quadratic regression of Equation (4) at nominal speed (ω0) with the pump affinity laws (5-7) using pump efficiency equation as a function of pump speed from reference [4] the following expression is obtained:

$$\eta_p = 1 - \left(1 - \eta_{p0}\right) \cdot \left(\frac{Q_0}{Q}\right)^{0.1} \quad (11)$$

$$\eta_p = 1 - [1 - D \cdot Q_n - E \cdot (Q_0)^2] \cdot \left(\frac{Q_0}{Q}\right)^{0.1} \quad (12)$$

(Q), the actual hydraulic power is obtained (Phid). By dividing the actual hydraulic power (Phid) with the actual pump efficiency (ηp), the pump shaft power (Ppump) is obtained [8]:

$$P_{pump} = P_{hid}/\eta_p \quad (15)$$

2.4 Induction Motor

The submersible pump is connected by a shaft at a 50 Hz, 3 phase (400V) induction motor [3] of 51 kW. The induction motor has 2 poles leading to an angular velocity of 2870 rpms. The current consumption by the motor is 101 A considering a 0.85 power factor, and a efficiency of 84%.

Table 4

Induction motor characteristics [3].

Induction motor data	**Symbol**	**Value**
IM nominal power	P_{IM0}	51 kw
IM efficiency	η_{IM0}	84 %
IM nominal frequency	f_r	50 Hz
IM nominal voltage	V_{IM}	400 V
IM nominal current	I_{IM}	101 A
IM number of poles	poles	2
IM rotor synchronous speed	ω_s	3000 rpm

IM rotor nominal speed	Ω_n	2870 rpm
IM rotor operating speed	ω_o	Variable
IM Power factor (cos φ)	cos φ	0.85
IM nominal efficiency	η_{IM}	84%

In the induction motor, the stator is composed of three windings 120º spatially shifted and one pair of poles. When these three stator windings are supplied by a balanced three phase voltage of frequency fs, the stator flux is induced. This stator flux rotates at constant speed. That is, the synchronous speed (ns) is given by the following expression [9]:

$$\omega_s = \frac{120 \cdot f_s}{poles} = 3000\, rpm \qquad (16)$$

The slip defines the relation between the nominal angular velocity of the stator and the rated angular velocity of the rotor [9]:

$$s = \frac{\omega_s - \omega_n}{\omega_s} = 4.33\% \qquad (17)$$

Considering the that the pump shaft is directly connected to the induction motor rotor, and ignoring the shaft torsion, it can be assumed that the speed of the pump is the same as the speed of the induction motor rotor. Due to this assumption, for the ratio of the between the rotor operating angular velocity (ω), and the nominal angular velocity (ω0), can be used the same denotation α, and the operating frequency is obtained according to the following expression [9]:

$$f_o = \frac{\alpha \cdot \omega_r \cdot poles}{120 \cdot (1-s)} \qquad (18)$$

The induction motor power is calculated:

$$P_{IM} = P_{pump}/\eta_{IM} \qquad (19)$$

2.5 Diesel Generator

Currently the irrigation system is powered by an old diesel generator of 60 kVA prime power, working at 400 Vac and a frequency of 50 Hz. From energy measurements during the nominal operating of the irrigation system, was found the pumping unit (induction motor and the submersible pump), operating at the nominal frequency 50 Hz consumes a current of 47.5 A at 400 V (cos φ=0.8) with the diesel generator consuming approximately 6 l/h of diesel according to the user.

Table 5

Diesel generator data.

Diesel generator parameter	Symbol	Value
Prime Power	P_{DG}	60 kVa
Operating frequency	f_{DG}	50 Hz
Current measurements during operation	I_{DG}	47.5 A
Nominal Voltage	V_{DG}	400 Vac
Power factor	cos φ	0.85
Diesel consumption according to datasheet workload 75%	$C_{Diesel75}$	8.4 l/h
Diesel consumption according to datasheet workload 100%	$C_{Diesel100}$	12 l/h

The workload of the diesel generator during the irrigation system operation, is calculated according to the following formula:

$$Workload = \frac{3 \cdot I_{DG} \cdot V_{DG}}{\sqrt{3} \cdot P_{DG}} = 54.848\,\% \quad (20)$$

The workload in kVA is:

$$P_{DGO} = workload \cdot P_{DG} = 32.909\, kVA \quad (21)$$

Upcoming, the active power of the diesel generator is obtained in equation (22):

$$P_{DGOA} = P_{GO} \cdot \cos\varphi = 27.973\, kW \quad (22)$$

Assuming a linear diesel consumption by the generator between the two working points given by the manufacturer (CDiesel75 and CDiesel100), the actual diesel consumption is estimated to be:

$$C_{DieselO} = Workload \cdot \frac{C_{Diesel75}}{75\%} = 6.143\, l/h \qquad (23)$$

Consumption confirmed by the user of the irrigation system. The diesel consumption for each kWh is estimated to be:

$$C_{Diesel-kWh} = C_{DieselO}/P_{DGOA} = 0.233\, l/kWh \qquad (24)$$

Considering a diesel consumption of 6.143 l/h by the diesel generator for operating a submersible pump that delivers 85 m^3/h, and total pumped volume every year of 177 442 m^3, by a pump, the annual diesel consumption is estimated according to the following formula (128823.852 liters of diesel for the water volume pumped with the existing system and 12824.141 liters of diesel for the volume pumped with the PV generator):

$$C_{Diesel/year} = \frac{177\,442}{85} \cdot C_{DieselO} = 12823.852\ l \quad (25)$$

3. INTEGRATING A HIGH-POWER PHOTOVOLTAIC GENERATOR

The integration of a photovoltaic generator into the existing irrigation system has very clear objectives:

- Hybridizing the existing expensive and polluting electricity source (diesel generator) of the irrigation system, with a clean photovoltaic generator.
- Automatization of the irrigation system in order to start up the irrigation whenever the photovoltaic generator electrical power production covers the minimum electrical power required by the irrigation system. it allows monitoring of the system through a remote application.
- Remote access for operating the irrigation system.
- Lower operating cost of a photovoltaic generator in comparison with the diesel generator.
- Reducing, even eliminating the CO2 emissions produced by diesel generator, contributing to environmental sustainability.

3.1 Variable frequency drive

In order to take advantage at maximum from the PV generator, a variable frequency drive (VFD) [10] will drive the AC induction motor also at partial load, when there is not enough power in the PV generator to run the motor at nominal power.

The VFD complies with IEC 61000-6-2 [11], IEC 61000-6-4 (EMI) [12] and EN50178 [13] standards and can operate in ambient temperature higher than 50ºC. Due to the reason that the maximum voltage of the system with the current configuration can exceed a voltage higher then 830Vdc at low temperatures, a contactor will be installed at the DC bus input to disconnect the DC bus connection from the PV generator.

Table 6

Variable frequency drive characteristics [10].

VFD data*	Symbol/Value
DC input	
Maximum voltage	980 Vdc
MMP voltage range	540-830 Vdc
Nr. DC inputs	1
Hybrid connection	Yes
AC output	
AC rated power	45 kW
AC rated voltage	400 V AC
AC rated frequency	50 Hz
EMC filter	Yes-C3
DV/Dt Filter	No
AC maximum continuous current	94 A
Losses	
No-load inverter losses [15]	k_0=0.0115
Linear inverter losses [15]	k_1=0.0015
Joule inverter losses [15]	k_2=0.0438

The variable frequency drive is characterized by its nominal (PVFD) and maximum output powers and three experimental parameters (k0, k1 and k2), which are associated, respectively, to the no-load, linear, and Joule inverter losses of the variable frequency drive. Based on these parameters, the electrical power required by the variable frequency drive efficiency will be calculated [14]:

$$\eta_{VFD} = \frac{p_{AC}}{p_{AC} \cdot (k0 + k1 \cdot p_{AC} + k2 \cdot (p_{AC})^2)} \quad (26)$$

Where pAC=PIM/PVFD.DC, with PIM the AC required by the induction motor and the PVFD.DC the VFD DC requested power [15]. The electrical power required by the VDF is:

$$P_{VFD.DC} = \frac{P_{IM}}{\eta_{VFD} \cdot \eta_{filter} \cdot \eta_{\Delta Vac}} \quad (27)$$

Where PIM is the electrical power required by the induction motor, ηVFD is the VFD efficiency, η_{filter} is the DV/DT filter efficiency, and $\eta_{\Delta Vac}$ is the efficiency including the loses due to the voltage drop in the AC cables (1-3%).

3.2 Solar tracker

The 171 photovoltaic panels are distributed on three decentralized self-operated horizontal single-axis trackers (HSAT) [16] (57 on each tracker). The trackers have N-S (north-south) orientation and a 110º range of motion around its axis.

The tracker structure it is made of galvanized hot-steel and complies with EN 1991 [17, 18] regarding the resistance to the loads created by the self-mass, snow and wind characteristics at the site location and with ISO 9223 [19] regarding the protection against corrosion.

A 5 meters distance between the trackers was determined to be the optimum distance for avoiding most of the shadows between the rows and allows access for cleaning and periodic inspection and maintenance.

The tracker control system controls the motor of the tracker and includes the algorithm for tracking the sun irradiation, the backtracking algorithm for avoiding the shadows from one tracker to another, and includes also protections and alarms regarding axis blockage (the tracker stops its movement when reaching ±55º, or if it detects more power consumption in rotating the tracker than usual) or wind speeds (the tracker goes in safe position if it detects wind speeds greater than the limit).

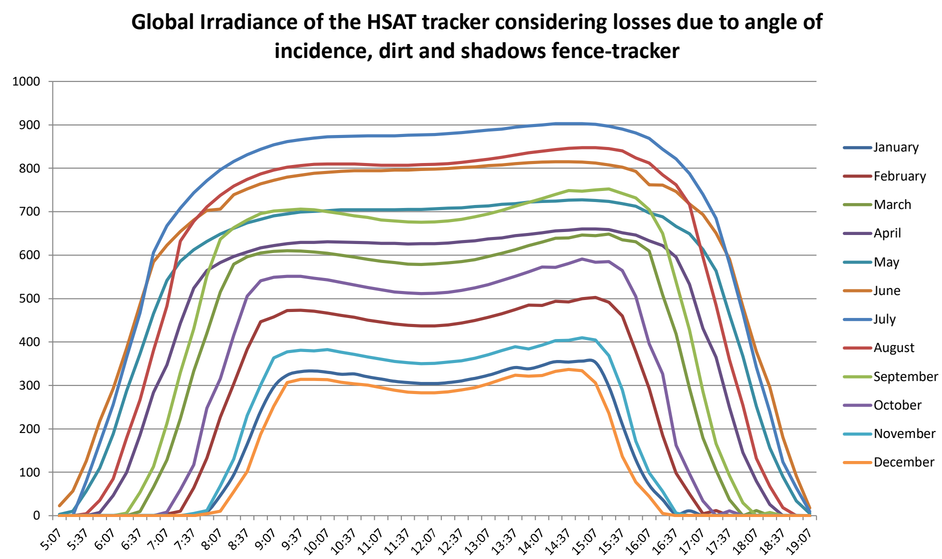

Fig. 3. Global Irradiance of the HSAT tracker considering losses due to angle of incidence, dirt and shadows fence-tracker.

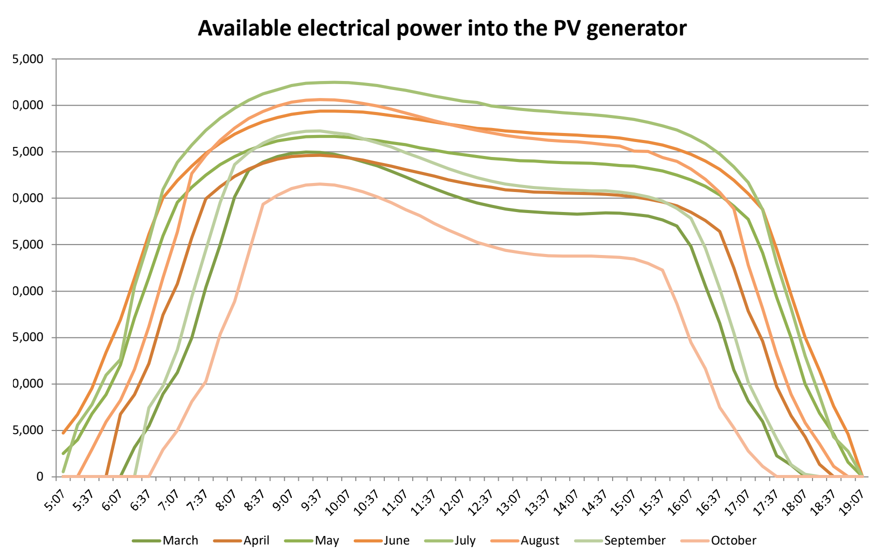

Fig. 4. PV generator available electrical power.

Table 7

Photovoltaic tracker characteristics [16].

Data*	Value
Dimensions	
PV Modules per beam	57
Installed power (PV module of 335 W)	56.95 kWp
Pv module height. Tracker in horizontal position 0	2 m
Pv module height. Tracker in 55 deg position	2.37 max, 0.4 min
Drive unit	
Drive unit type	Electromechanical rotary actuator
Drive unit power supply	155 W / 24 DC – Self-powered
Mechanical characteristics	
Rotating range	Up to +/- 55º
Maximum wind speed in horizontal position	140 km/h
Control system	
Tracking controller	Astronomical Algorithm
Backtracking Management	Backtracking Algorithm
Wind Management	User-configurable feathering table
Tilt sensor	Inclinometer
Considered dirt factor (%D)	0.22

Table 9

Photovoltaic panel characteristics [24].

Photovoltaic panel data*	Symbol	Value
Peak Power Watts	P_{MAX}	335 Wp
Power Output Tolerance	-	0/+5
Maximum Power Voltage	V_{MPP}	37.4 V
Maximum Power Current	I_{MPP}	8.96 A
Open Circuit Voltage	V_{OC}	45.9 V
Short Circuit Current	I_{SC}	9.45 A
Module Efficiency	η_{PV}	16.9 %
Nominal Operating Cell Temperature	NOCT	44°C
Temperature Coefficient of PMAX	K_P	-0.41%/K
Temperature Coefficient of VOC	K_V	-0.32%/K
Temperature Coefficient of ISC	K_I	0.05%/K
Initial PV module power loss	η_{PPV}	3%
Yearly PV module power loss	$\eta_{PPVyear}$	0.7%

**Electrical data at standard conditions (Irradiance 1000 W/m², Cell Temperature 25 °C, Air Mass AM1.5)*

Table 8

Irradiation data at site location from PVGIS 5.2

Parameter	Symbol	Units
Global irradiation	G_{global}	W/m^2
Diffuse irradiation	G_{diff}	W/m^2
Clear sky irradiation	$G_{clearsky}$	W/m^2
Environment temperature	T_{env}	ºC
Direct irradiation	G_{direct}	W/m^2
Solar time	H	hh:mm

The irradiation data from Table 8 at the site location was obtained from PVGIS 5.2 [20].

The global irradiance reaching the PV generator considering the losses due to the angle of incidence, the dirt (dust) on the PV panels and the shadows created by the fence is presented in Figure 3, and was calculated according to references [21, 22, 23].

3.3 Photovoltaic generator

The photovoltaic generator (56.95 kW) consists of 170 photovoltaic panels of 335 W [24], combined in 10 strings of 17 photovoltaic panels in series (5.695 kW) powering the pumping system. Another photovoltaic panel of 335 W [24] is used for powering the control unit.

The cell temperature of the PV generator is calculated using equation:

$$T_{cell} = T_{env} + (NOCT - 20^0C) \cdot \frac{G_{\beta G}}{800} \quad (55)$$

The PV generator produced power is calculated using equation:

$$P_{PVG} = (P_{MAX} \cdot \eta\text{PPV}) \cdot G_{\beta G} \cdot [1 - K_V(T_{cell} - 25^0C)] \cdot K_P \cdot \eta_{\Delta dc} \quad (56)$$

Where ηΔVac is the efficiency including the loses due to the voltage drop in the DC cables (1-1.38%).

4. RESULTS

Based on the PV generated power from equation 56 and Figure 4, the pumped volume flow into the irrigation system it is presented in Table 10. By comparing water volume pumped into the irrigation system with the PV generator (Table 8) with water volume pumped into the irrigation system by the actual system (Table 2), PV generator covers the entire volume required by the irrigation system during the entire year:

$$\frac{177\ 446\ \mathrm{m}^3}{177\ 442\ m^3} = 100\%. \qquad (58)$$

5. FINANCIAL ADVANTAGE OF THE PROPOSED SOLUTION

Considering a total consumption of 12824.141 of diesel consumption per year for pumping 177 446 m^3 of water into the irrigation system, and assuming a price of 1 euro/liter of diesel for agricultural use (not including the road tax), the annual cost of operation for the actual system is 12824.141 euros.

Assuming a total investment of 100 000 euros for integrating the high-power photovoltaic generator and to automate the entire irrigation system, the payback period is 7.8 years (100 000 €/ 12 825€). The obtained payback period doesn't take into consideration the replacement cost of the diesel generator and assumes that the diesel generator still has the same lifetime expectancy as the PV generator (more than 20 years). The remaining 12.2 years (expected lifetime of the PV generator 20 years – payback period 7.8 years) will bring a profit of 156 465 euros.

Table 10

Water volume pumped into the irrigation system with the PV generator.

Month	Water volume pumped each day with the PV generator	Water volume pumped each month with the PV generator
January	0	0
February	180.09	5 042
March	576.83	17 882
April	690.35	20 711
May	747.56	23 174
June	826.74	24 802
July	835.98	25 915
August	767.98	23 807
September	661.75	19 853
October	524.49	16 259
November	0	0
December	0	0
Total volume		177 446 m^3

6. CONCLUSION

Finally, it can be concluded that integration of a photovoltaic generator into the existing irrigation system has very clear objectives has a payback period of 7.8 years, assuming a constant price of the diesel for agricultural purpose at 1 euro/liter, and the same lifetime expectancy as the PV generator. The profit at the end of the project will be of 156,465 euros. Besides the economic and financial profitability, other benefits brought by the high-power PV generator integration into the studied irrigation system are:

1. The automatization of the irrigation system in that it is monitored and controlled remotely.
2. Lower maintenance cost of a photovoltaic generator in comparison with the diesel generator.
3. Eliminating the CO2 emissions produced by diesel generator, contributing to environmental sustainability

7. REFERENCES

[1] Yang, Z.; Soleiman, K.; Løhndorf, B. *Energy Efficient Pump Control for an Offshore Oil , System.* IFAC ACOOG, 45, 257–262.

[2] M. Bărglăzan, C. Velescu, T. Miloş, A. Manea, E. Dobândă & C. Stroiţă., *Hydrodynamic Transmission Operating With Two-phase Flow,* Computational Methods in Multiphase Flow IV, WIT Transactions on Engineering Sciences, ISSN 1743-3533 Vol 56, 2007.

[3] Caprari, *Submersible Electric Pump E8P95/7ZC+MAC870-8V Technical Data Sheet. 2019.* Available online: https://ipump.caprarinet.net/ (accessed on 9 October 2021).

[4] Sarasúa, J.I.; Martínez-Lucas, G.; Platero, C.A.; Sánchez-Fernández, J.Á. *Dual Frequency Regulation in Pumping Mode in a Wind–Hydro Isolated System.* Energies 2018, 11,2865.

[5] Sârbu, I.; Borza, I. *Energetic optimization of water pumping in distribution systems.* Period. Polytech. Ser. Mech. Eng. 1998, 42 141–152.

[6] Daniel Catalin Stroita, Adriana Sida Manea*, Anghel Cernescu, *Blade Polymeric Material Study of a Cross-Flow Water Turbine Runner,* MATERIALE PLASTICE Vol. 56 No. 2, 2019

[7] White, F.M. *Chapter 11 Turbomachinery. In Fluid Mechanics*, 7th ed.; McGraw-Hill: New York, NY, USA, 2011; pp. 776–777.

[8] Tokar, Dănuț & Stroita, Daniel Catalin & Tokar, Adriana & Rusen, Alexandra. *Hybrid System that Integrates the Lost Energy Recovery on the Water-Water Heat Pump Exhaust Circuit*. IOP Conference Series: Materials Science and Engineering. 603. 042002. 10.1088/1757-899X/603/4/042002, 2019

[9] Abad, G.; López, J.; Rodríguez, M.A.; Marroyo, L.; Iwanski, G. *Doubly Fed Induction Machine: Modeling and Control for Wind Energy Generation*; John Wiley & Sons: Hoboken, NJ, USA, 2011; pp. 155–238.

[10] Nidec Control Techniques, *Powerdrive F300* Nidec Control Techniques Ltd, The Gro Newtown Powys SY16 3BE UK, p. 324, 2017.

[11] *EN IEC 61000-6-2:2019* Electromagnetic compatibility (EMC) - Part 6-2: Generic standards - Immunity standard for industrial environments

[12] *EN IEC 61000-6-4: 2019* Electromagnetic compatibility (EMC) - Part 6-4: Generic standards - Emission standard for industrial environments

[13] *EN 50178* Electronic equipment for use in power installations - European Standard

[14] M. Jantsch, H. Schmidt, J. Schmid. *Results of the concerted action on power conditioning and control*. 11th European Photovoltaic Solar Energy Conference 1992: 1589-1592.

[15] Muñoz, J., Martínez-Moreno, F. and Lorenzo, E. (2011), *On-site characterisation and energy efficiency of grid-connected PV inverters*. Prog. Photovolt: Res. Appl., 19: 192–201.

[16] STI Norland, *STI-H250 Horizontal Single Axis Tracker – Technical Data* https://www.stinorland.com/es, 2017

[17] *EN 1991-1-1*: Eurocode 1: Actions on structures - Part 1-1: General actions - Densities, self-weight, imposed loads for buildings

[18] *EN 1991-1-4:2005* Wind actions - Eurocodes

[19] *ISO 9223:2012* Corrosion of metals and alloys — Corrosivity of atmospheres — Classification, determination and estimation

[20] European Comission, *PVGIS 5.2 PHOTOVOLTAIC GEOGRAPHICAL INFORMATION SYSTEM,* available online at: https://re.jrc.ec.europa.eu/pvg_tools/en/

[21] MASLOWATEN, *Technical Specifications for PV irrigation systems*, 2007. [Online]. Available: http://maslowaten.eu/?page_id=57&lang=es.

[22] Narvarte, L. & Pigueiras, Eduardo. (2008). *Tracking and Ground Cover Ratio*. Progress in Photovoltaics: Research and Applications. 16. 703 - 714. 10.1002/pip.847.

[23] Pigueiras, Eduardo & Narvarte, L. & Munoz, J.. (2011). *Tracking and back-tracking*. Progress in Photovoltaics: Research and Applications. 19. 747–753. 10.1002/pip.1085.

[24] Trina Solar, *144 cell multicrystalline photovoltaic module 335–345w power* available online at: www.trinasolar.com, 2017.

Studiu privind implementarea unei soluții alternative la un sistem actual de irigații

Rezumat: În această lucrare este prezentat un studiu tehnic și economic pentru integrarea unui generator fotovoltaic de mare putere într-un sistem de irigare. În prima parte este prezentată modelarea fiecărei componente a sistemului de irigare existent (rețeaua hidraulică, pompă submersibilă, motorul cu inducție și generator diesel). În a doua parte, este prezentată modelarea unui generator de mare putere pe un tracker solar cu o axă orizontală orientată N-S. În ultima parte, s-a calculat perioada de amortizare a generatorului fotovoltaic de mare putere, raportat doar la prețul combustibilului folosit de generatorul diesel pentru extragerea și pomparea aceluiași volum de apă.

Dorin BORDEASU, Ph.D., Student, Politehnica University of Timisoara, Department of Automation and Applied Informatics, bordeasu.dorin@student.upt.ro, +40771457276, Timisoara, Romania.